Structure Determination of a DNA Octamer in Solution by NMR Spectroscopy. Effect of Fast Local Motions†

T. M. G. Koning,‡ R. Boelens,‡ G. A. van der Marel,§ J. H. van Boom,§ and R. Kaptein*,‡

Department of Chemistry, University of Utrecht, Padualaan 8, 3584 CH Utrecht, The Netherlands, and Gorlaeus Laboratory, State University of Leiden, P.O. Box 9502, 2300 RA Leiden, The Netherlands

Received June 22, 1990; Revised Manuscript Received October 4, 1990

ABSTRACT: NMR structures of biomolecules are primarily based on nuclear Overhauser effects (NOEs) between protons. For the interpretation of NOEs in terms of distances, usually the assumption of a single rotational correlation time corresponding to a rigid molecule approximation is made. Here we investigate the effect of fast internal motions of the interproton vectors in the context of the relaxation matrix approach for structure determination of biomolecules. From molecular dynamics simulations generalized order parameters were calculated for the DNA octamer d(GCGTTCGC)·d(CGCAACGC), and these were used in the calculation of NOE intensities. The magnitudes of the order parameters showed some variation for the different types of interproton vectors. The lowest values were observed for the interresidue base H6/H8–H2″ proton vectors (S^2 = 0.60), while the cytosine H5–H6 interproton vectors were among the most motionally restricted (S^2 = 0.92). Inclusion of the motion of the interproton vectors resulted in a much better agreement between theoretically calculated NOE spectra and the experimental spectra measured by 2D NOE spectroscopy. The interproton distances changed only slightly, with a maximum of 10%; nevertheless, the changes were significant and resulted in constraints that were better satisfied. The structure of the DNA octamer was determined by using restrained molecular dynamics simulations with H_2O as a solvent, with and without the inclusion of local internal motions. Starting from A- or B-DNA, the structures showed a high local convergence (0.86 Å), while the global convergence for the octamer was ca. 2.6 Å.

A variety of three-dimensional structures for biomolecules in solution have been determined during the last decade. Since these structures are primarily based on distance information from nuclear Overhauser spectroscopy (Wüthrich, 1986, 1988; Kaptein et al., 1988; Clore & Gronenborn, 1989), considerable attention has been focused on improving the interpretation of NOE intensities. Several approaches based on the full relaxation matrix (Bothner-By & Noggle, 1979; Keepers & James, 1984; Olejniczak et al., 1986; Marion et al., 1987; Lefèvre et al., 1987; Boelens et al., 1988, 1989; Summers et al., 1990) have been suggested in order to compensate for spin diffusion effects, which form a serious source of errors in the distance determination for larger biomolecules. All methods have in common that a cross-relaxation rate matrix **R** is calculated on the basis of a starting structure after which the familiar set of generalized Bloch equations is solved.

This set of coupled differential equations can be solved either by diagonalization of the matrix **R** (Keepers & James, 1984; Boelens et al., 1988, 1989) or by stepwise integration (Marion et al., 1987; Lefèvre et al., 1987). The calculated NOE intensities can be compared with the experimental ones, and the structure can be varied until the correspondence between the two sets is satisfactory. Boelens et al. (1988, 1989) have proposed an iterative procedure in which the variation of the structural models is based on the distance constraints obtained after a back transformation of a mixed NOE matrix. The mixed matrix consists of both theoretical and experimental NOE intensities. It was demonstrated for a DNA octamer that both the distance determination and the structure determination improved compared to a two-spin analysis of the available NOE data. This approach was shown to be successful for structure determination of DNA fragments (Boelens et al., 1989; Pieters et al., 1990) and also for proteins (Rullmann et al., 1990).

In the calculation of the cross-relaxation matrix, the molecules have been treated so far as rigid bodies undergoing only overall motion with a single correlation time τ_0. However, internal motion can affect the correlation times locally, especially in mobile parts of larger molecules. This change in τ_0 due to motion will result in changes in ^{13}C relaxation parameters (Levy et al., 1981) or, with respect to the ^1H NOEs, in changes in the cross-relaxation rates. This was shown for lysozyme (Olejniczak et al., 1984) where the NOE data for a number of protons, even of buried residues in the protein, did not fit the rigid-model assumption. A much better description was obtained when a molecular dynamics simulation was used to predict the motional behavior.

In DNA, where the bases are known to have correlation times different from the sugar, the same problems may be expected. Several methods have been suggested to incorporate the effect of local motion in the interpretation of the NOE intensities. One of the approaches was to choose three different correlation times: (1) one for all the sugar–sugar and sugar–base cross peaks not involving H2′ and H2″ or methyl groups, calibrated with the cytosine H5–H6 contact, (2) one for all the cross peaks where H2′ and H2″ were involved, calibrated with the H2′–H2″ contacts, and (3) one for all the cross peaks where methyl groups play a role, calibrated with thymine H6–Me (Clore & Gronenborn, 1985a). Another approach consisted of the use of different overall correlation times in the calculation of NOE intensities with a full relaxation matrix approach (Broido et al., 1985; Jamin et al., 1985). A better fit of the NOE data was obtained when small variations in the overall correlation time were allowed. Recently,

† This research was supported by The Netherlands Foundation for Chemical Research (SON) with financial aid from The Netherlands Organization for the Advancement of Research (NWO).

* Author to whom correspondence should be addressed.
‡ University of Utrecht.
§ State University of Leiden.

0006-2960/91/0430-3787$02.50/0

Lancelot et al. (1989) also observed a better correspondence between experimental and calculated intensities when, for the interproton vectors to the H2′ and H2″, extra effective correlation times were added in the Woessner equation (Woessner, 1962).

Here we present an approach to include the effect of fast internal motion in the interpretation of the NOE intensities for DNA in the framework of the iterative relaxation matrix approach (IRMA). A long molecular dynamics (MD) simulation of the DNA molecule in water and in the presence of counterions was used to extract the generalized order parameters that reflect local changes in correlation times. These generalized order parameters were used both in the calculation of the theoretical NOE intensities and in the back-transformation to proton–proton distances, which are in turn used for structure refinement. Previously, similar MD simulations were used to calculate ^{13}C relaxation times (Levy et al., 1981) and ^{1}H NOEs in lysozyme (Olejniczak et al., 1984). The procedure will be applied to the DNA octamer d-(GCGTTGCG)·d(CGCAACGC), which has served previously as a test case for the IRMA procedure (Boelens et al., 1989). The numbering of the residues is shown in model 1. The 2D NOE spectrum of this octamer has been assigned by Kemmink et al. (1987).

```
     1        8
5'  GCGTTGCG  3'
3'  CGCAACGC  5'
    16       9
```

model 1

The effect of inclusion of fast internal motion on the correspondence between theoretical and experimental NOEs will be expressed in terms of R factors. Inclusion of the local mobility in the calculations is shown to improve the R factors, and it also affects the NOE-derived proton–proton distances and the structures determined with these distances.

Finally, a protocol for the incorporation of this type of fast internal motion in conjunction with IRMA is proposed for the structure refinement of biomolecules. In this method a full relaxation matrix calculation is combined with free MD simulations and restrained MD (Kaptein et al., 1985; Brünger et al., 1986; Nilges et al., 1988).

Theory

In this section the theory that allows us to describe the effect of picosecond internal motion on the cross-relaxation rates will be described. Furthermore, the extraction of information about fast local motion from a molecular dynamics trajectory is discussed. Macura and Ernst (1980) have shown that the normalized intensities of a 2D NOE spectrum recorded with a mixing time τ_m are given by the elements of an exponential matrix:

$$I_{ij} = [e^{-\mathbf{R}\tau_m}]_{ij} \tag{1}$$

where $\mathbf{R}$ is a relaxation matrix with diagonal elements

$$\rho_i = R_{ii} = \frac{2\pi}{5}\gamma^4\hbar^2 \sum_{j=1,j\neq i}^{N} [J_{ij}^0(\omega) + 3J_{ij}^1(\omega) + 6J_{ij}^2(\omega)] + R_{\text{leak}} \tag{2}$$

and the off-diagonal elements of $\mathbf{R}$ contain the cross-relaxation rate

$$\sigma_{ij} = R_{ij} = \frac{2\pi}{5}\gamma^4\hbar^2[6J_{ij}^2(\omega) - J_{ij}^0(\omega)] \tag{3}$$

where γ is the proton gyromagnetic ratio and ω is the ^{1}H Larmor frequency. When all the interproton vectors are assumed to be rigid and to move isotropically, the spectral density functions take the form (Solomon, 1955)

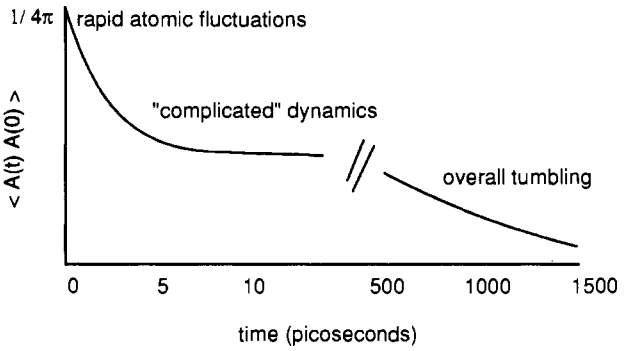

FIGURE 1: Idealized description of the time course of the correlation function for internal motions.

$$J_{ij}^n(\omega) = \frac{1}{4\pi r_{ij}^6}\left[\frac{\tau_0}{1 + (n\omega\tau_0)^2}\right] \tag{4}$$

where τ_0 is the overall rotation correlation time and r_{ij} is the distance between proton i and proton j. When anisotropic fast internal motions are taken into account, the spectral density functions change. To describe systems where overall and fast internal motions occur, the model-free approach proposed by Lipari and Szabo (1982) can be used. The model-free approach describes systems in terms of the rate of overall and internal motions (correlation time τ_p) and a generalized order parameter S^2. S^2 varies between 0 and 1, the former corresponding to completely isotropic motion and the latter to the absence of local motion (rigid model). The generalized order parameter can be determined from the time correlation function of the interproton vector. The time correlation function is described by

$$C(t) = \left\langle \frac{A(t)A(0)}{r_{ij}^3(t)r_{ij}^3(0)} \right\rangle \tag{5}$$

where $A(t) = Y_n^2[\Phi_{\text{lab}}(t)]$ is the second-order spherical harmonics and $\Phi_{\text{lab}}(t)$ specifies the orientation of the interproton vector relative to an external magnetic field. The general form of such a time correlation function is shown in Figure 1. After a rapid initial decay that is due to the fast internal motion, a plateau value is reached in a time τ_p of the order of a few picoseconds. On a much longer time scale (nanosecond range) the function decays to zero due to overall motions of the molecule. It is the plateau value of the normalized correlation function to which the generalized order parameter is related:

$$C(t) = \left\langle \frac{A(t)A(0)}{r_{ij}^3(t)r_{ij}^3(0)} \right\rangle = S^2\langle r_{ij}^{-6}\rangle \qquad \text{for } t > \tau_p \tag{6}$$

The time correlation function can now be rewritten in another form:

$$C(t) = \frac{1}{4\pi}[S^2\langle r_{ij}^{-6}\rangle + (1 - S^2)\langle r_{ij}^{-6}\rangle \exp(-t/\tau_p)] \tag{7}$$

where the first part describes the plateau and the second part describes the decay with the correlation time τ_p to the plateau value $S^2\langle r_{ij}^{-6}\rangle$. When, in addition, overall isotropic motion with a correlation time τ_0 occurs, the correlation function has the form

$$C(t) = \frac{1}{4\pi}[S^2\langle r_{ij}^{-6}\rangle \exp(-t/\tau_0) + (1 - S^2)\langle r_{ij}^{-6}\rangle \exp(-t/\tau_c)] \tag{8}$$

where $\tau_c^{-1} = \tau_0^{-1} + \tau_p^{-1}$.

The spectral density functions, being the cosine Fourier transforms of the time correlation functions, are given by

$$J_{ij}^n(\omega) = \frac{1}{4\pi}\left[S^2\langle r_{ij}^{-6}\rangle\frac{\tau_0}{1+(n\omega\tau_0)^2} + (1-S^2)\langle r_{ij}^{-6}\rangle\frac{\tau_c}{1+(n\omega\tau_c)^2}\right] \quad (9)$$

If now the internal motions are in the motional narrowing limit ($\omega\tau_c \ll 1$), the spectral density functions are

$$J_{ij}^n(\omega) = \frac{1}{4\pi}\left[S^2\langle r_{ij}^{-6}\rangle\frac{\tau_0}{1+(n\omega\tau_0)^2} + (1-S^2)\langle r_{ij}^{-6}\rangle\tau_c\right] \quad (10)$$

Furthermore, when the internal motions are very fast compared to the overall motion ($\tau_p \ll \tau_0$), the second term of eq 10 can be neglected, and the spectral density functions are uniformly reduced to

$$J_{ij}^n(\omega) = \frac{S^2\langle r_{ij}^{-6}\rangle}{4\pi}\left[\frac{\tau_0}{1+(n\omega\tau_0)^2}\right] \quad (11)$$

Equation 11 can be used with eqs 2 and 3 to calculate the relaxation rates and the NOE intensities.

Experimental Procedures

Experimental. The complementary strands d-(GCGTTGCG)·d(CGCAACGC) were synthesized via a phosphotriester approach (van der Marel et al., 1981; van Boom et al., 1982) and mixed in a 1:1 ratio to form the duplex. Solutions were 70 mg/mL duplex in 50 mM KP_i and 0.2% NaN_3, pH 6.5 (meter reading), in ^2H_2O. Spectra were recorded at 300 K.

Eight 2D NOE spectra were recorded at 50 MHz with a Bruker WM 500 spectrometer equipped with an Aspect 2000 computer. Phase-sensitive spectra were obtained by using phase cycling as described by States et al. (1982). Mixing times were 6.6, 10.5, 16.7, 26.8, 42.9, 68.7, 110, and 176 ms. The spectra were Fourier transformed on a DEC microVAX II with the "2D NMR" software library, written in Fortran 77. The same parameters were used for all mixing times and a baseline correction was applied in the ω_1 domain. The cross peaks in all the 2D NOE spectra of the time series were integrated by summation of the intensity in an area around the cross peak.

Free MD Simulation. All the energy minimization and molecular dynamics simulations were performed by using the GROMOS force field and programs (van Gunsteren & Berendsen, 1987). In this force field only polar protons were treated explicitly. The other protons were incorporated by using the united atom technique.

For the free MD simulation an energy-minimized canonical B-DNA structure for the DNA octamer was put in a rectangular box containing 1241 water molecules and 14 sodium ions, which compensated the negative charges on the phosphate backbone. The whole system was subjected to an energy minimization to remove the unfavorable electrostatic interactions introduced by adding water and ions. For the atoms in this system initial velocities for the MD run were taken from a Maxwellian distribution at 300 K. The system was simulated for 200 ps. The time step was 2 fs, and the time constant for coupling to a thermal bath of 300 K was 10 fs during the first 10-ps equilibration period and 100 fs for the rest of the run. Periodic boundary conditions were applied and a cutoff of 8 Å was used; the nonbonded pair list was updated every 10 steps. The coordinates of the DNA were saved every 25 steps starting at 20 ps, and these trajectories were used for analysis. The root-mean-square atom positional fluctuations were calculated for the whole 180-ps trajectory and for nine subsets of 20 ps each. For this calculation the coordinates of each time frame were superimposed on the first by a translational and rotational least-squares fit for all the 16 C1′ atoms.

The time correlation functions $C(t)$, eq 5, for all the proton–proton vectors shorter than 5 Å were calculated by using a fast Fourier transform algorithm. Since not all the protons were simulated, they were generated for each configuration in a standard way. The three methyl protons were treated as a pseudoatom at the center-of-mass position of the three protons. The plateau value of the time correlation functions were determined by averaging the value of the functions $C(t)$, ignoring the first decay and the last part where Fourier transform artifacts play a role. Three different sets of generalized order parameters were calculated. The first set was based on the plateau values of the time correlation functions calculated for the trajectory from 20 to 200 ps. The second set was calculated for the trajectory from 20 to 40 ps, and the third set of order parameters was calculated by averaging the S^2 values that were derived from the nine trajectories of 20 ps.

IRMA Calculations. The IRMA procedure has been described in detail previously (Boelens et al., 1988, 1989). The new element is the inclusion of fast local motions. Here only a brief description of the procedure will be given. For the IRMA calculations an energy-minimized B-DNA structure was used as the starting structure. On the basis of the interproton distances, the spectral density functions were calculated either with eq 4 for the rigid molecule assumption or with eq 11, which includes the effect of picosecond motions. The correlation time for the overall tumbling was taken to be 3 ns, and the diagonal leakage rate was 1 s^{-1}. It should be noted that eq 11 contains the average proton–proton distance to the sixth power. In these calculations the sixth power of the actual distance is used. For the methyl groups fast rotation was taken into account by using an $\langle r^3\rangle$ averaging for the three methyl proton positions. Furthermore, an extra diagonal leakage rate, arising due to the fast rotation, was added (Koning et al., 1990). The cross-relaxation matrix elements were calculated, cf. eq 3, and, from these, eight NOE intensity matrices with the same mixing times as those of the experiment (see above) were obtained. These theoretical NOE matrices were used in a comparison between theory and experiment and to supplement the experimental NOE matrices in order to allow a back-transformation to the relaxation matrices from which proton–proton distances were then derived. The eight obtained cross-relaxation rate matrices were averaged, and the standard deviation was used in the calculation of upper and lower bound distance constraints. Distances from the relaxation matrices were obtained by using either eq 4 or eq 11. The upper and lower bounds for the 190 distance constraints were based on the experimental errors only (Boelens et al., 1989) and were directly used in a restrained molecular dynamics structure refinement calculation. No additional correction factors were added. In the restrained MD calculations the distances were entered via an extra harmonic pseudopotential defined as (Kaptein et al., 1985)

$$V_{dc} = \begin{cases} (1/2)K_{dc}(r_{ij} - r_{ij}^l)^2 & 0 \le r_{ij} \le r_{ij}^l \\ 0 & r_{ij}^l < r_{ij} < r_{ij}^u \\ (1/2)K_{dc}(r_{ij}^u - r_{ij})^2 & r_{ij}^u \le r_{ij} \end{cases} \quad (12)$$

where r_{ij} is the actual distance between atoms i and j in a

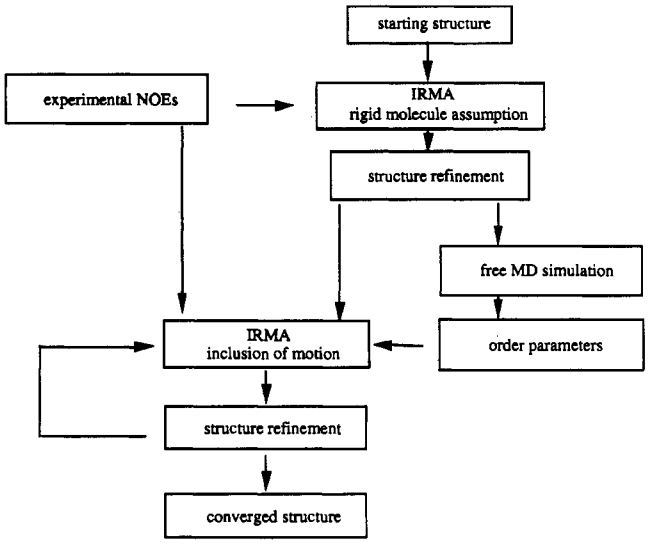

FIGURE 2: Protocol for structure determination of biomolecules taking into account the effect of fast local mobility.

structural model and r_{ij}^{u} and r_{ij}^{l} are the upper and lower bound constraints between atoms i and j. When the distance is either too short or too long compared to the constraint, this gives rise to extra potential energy (distance restraint energy, E_{dr}), and a force will be exerted on the proton pair. The force constant for the distance constraints (K_{dc}) was 4000 kJ·mol^{-1}·nm^{-2}. The restrained MD simulations were done in vacuo and the charges of the phosphates were neutralized. The other conditions were similar to those of the free MD run described above.

A Protocol for Structure Refinement. A protocol for structure refinement of biomolecules that takes into account the effect of fast local motions is shown in Figure 2. A starting model, which can be (1) an X-ray structure, (2) a structure obtained, for instance, with distance geometry and crude NOE constraints, or (3) a linear polypeptide chain, serves as input for a first IRMA cycle without inclusion of fast internal motion. The structure obtained is then used in a refinement step consisting of either restrained MD or a combination of distance geometry and restrained MD. The structure obtained in this way is first used in a free MD simulation for calculation of the order parameters and then in a new IRMA calculation with inclusion of fast motions through the order parameters. A structure refinement step is carried out again, and these last two steps can be repeated until a converged structure is obtained.

In our case an energy-minimized B-DNA structure was used as a starting structure for the "conventional" IRMA cycle, with only one overall correlation time of 3 ns. The derived distance constraints were used in a short restrained MD simulation of 15 ps. The average of the last 10 ps of this run was used as a starting structure for the next IRMA cycle. In this cycle, however, generalized order parameters are taken into account. These order parameters were obtained from a free MD simulation of 42.5 ps where the structure obtained from the first short MD run serves as a starting point. The first 2.5 ps of this run were used for equilibration, while the time correlation functions were calculated for the two 20-ps trajectories, and the obtained plateau values were averaged. In the newly derived set of distance constraints, both the effects of spin diffusion and of picosecond internal motions are taken into account. These constraints are then used in a 15-ps restrained MD run. The average of the last 10 ps was used as a starting structure for a final IRMA cycle where again the order parameters obtained as described above were used in the calculation of the distances and 15-ps restrained MD was performed for a final structure refinement. For all the MD simulations during this procedure, the DNA molecules were put in a box containing about 1300 water molecules and counterions. The same procedure was repeated with a canonical A-DNA model.

R Factor Calculation. A good way to judge the quality of the results is a direct comparison of the theoretically calculated, A_{ij}^{th}, and the experimental, A_{ij}^{exp}, NOE intensities. This can be done by using the R factor defined by Gonzalez et al. (1991):

$$R = \frac{\sum_{i,j}\sum_{\tau_m}|A_{ij}^{exp}(\tau_m) - A_{ij}^{th}(\tau_m)|}{\sum_{i,j}\sum_{\tau_m}A_{ij}^{exp}(\tau_m)} \quad (13)$$

where the summation runs over all measured intensitites (i,j) and all eight mixing times.

Simulation of the Spectra. Another way of comparing the theoretically calculated intensities is by simulation of the spectrum and visual inspection of both simulated and experimental spectra. For the simulation, the spectral intensities were taken from the calculated NOE matrix. The line widths were taken to be 15 Hz for the methyl proton lines and 30 Hz for all the others. For the chemical shift positions the assignments according to Kemmink et al. (1987) were used. All the lines were assumed to have a pure Lorentzian form. The spectra were stored in such a way that programs from the 2D NMR software library could be used to display and plot the spectra.

Analysis of the Structures. For the analysis of the obtained DNA structures, the program CURVES (Lavery & Sklenar, 1989) was used.

Results and Discussion

Free Molecular Dynamics Simulation. A free molecular dynamics simulation was performed in order to gain insight about the local mobility in the DNA molecule. Some parameters related to this mobility will be analyzed.

Atom Positional Fluctuations. Figure 3 shows plots of root-mean-square (rms) atomic fluctuations for some different atom types obtained from the MD simulation for the 180-ps trajectory and by averaging over 20-ps intervals. It is clear from this figure that for the 180-ps trajectory the magnitudes of the fluctuations are larger than for the 20-ps intervals, although the overall appearance of the curves does not change. This was also observed by Tidor et al. (1983) in both a molecular and harmonic dynamics simulation of a DNA hexamer. The explanation of this phenomenon is that in the DNA two types of motion are superimposed, short-time local fluctuations and longer time motions affecting a larger part or the whole molecule.

Various types of atoms were chosen in order to investigate the mobility in the backbone, sugar, and base regions of the DNA. The phosphate atoms showed the largest fluctuations, both short and long range (cf. Figure 3d), reflecting a large degree of motional freedom of the backbone. For the other atom types the base atoms, N3 for pyrimidine and N1 for purine, showed slightly less motion than the sugar when calculated over the whole 180-ps trajectory, but no difference could be observed when the 20-ps subsets were averaged. Both sugar atoms, C1′ and C2′, displayed about the same size of fluctuations, with the C2′ slightly more mobile than the C1′. This picture of different degrees of motion for the different parts of the molecule is consistent with the results of an earlier MD simulation of this octamer in water (van Gunsteren et al.,

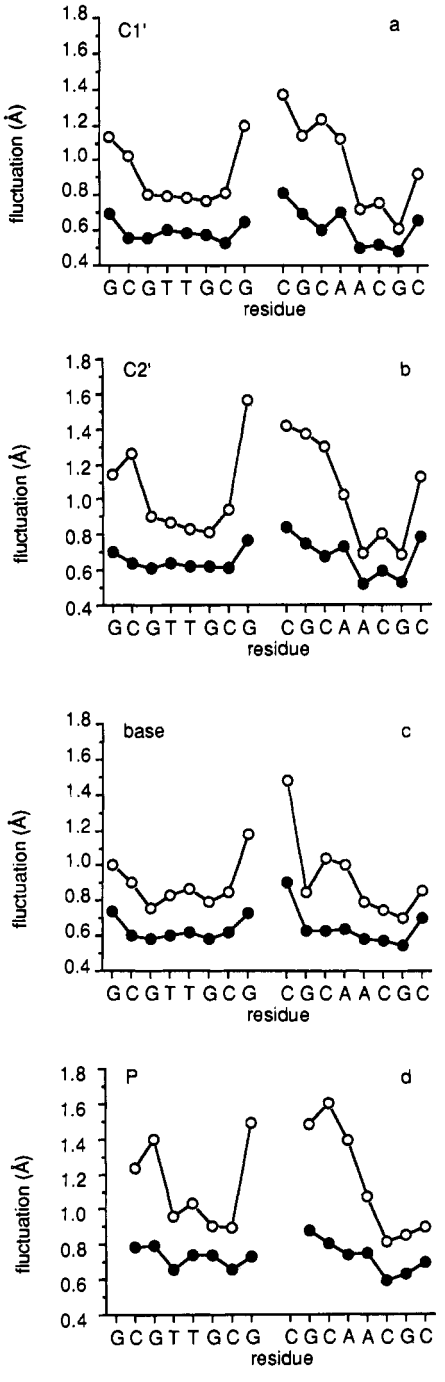

FIGURE 3: Root-mean-square atom positional fluctuations (Å). The fluctuations for different types of atoms in each residue for (○) for the 180-ps time span and for (●) a 20-ps time span are shown. (a) C1′ sugar atoms, (b) C2′ sugar atoms, (c) base N1 (purine) and N3 (pyrimidine) atoms, and (d) P backbone atoms.

1986) and with X-ray studies for the Dickerson dodecamer (Drew et al., 1981; Fratini et al., 1983). In the crystal, however, the difference in *B* factors for the sugar and the base atoms is larger than the spread in fluctuations of this simulation.

Another interesting feature is the overall form of the curves. For all the atoms in the second strand, the 5′ end showed much more flexibility than the 3′ end, and there is a drastic change when going down along the chain. This was also observed for the fluctuation on the 20-ps time scale. In the first strand six bases in the middle showed the same rigidity, and only the two bases at the end were more flexible. This may reflect a sequence-dependent variation in mobility. The large fluctuation

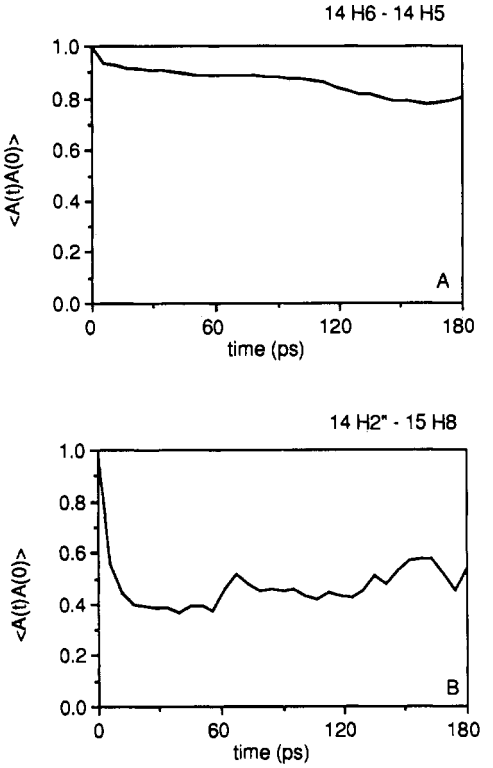

FIGURE 4: Decay of the internal motion correlation function over the 180-ps time span (A) for the fixed distance C14 H6–C14 H5 interproton vector and (B) for the interresidue C14 H2″–G15 H8 interproton vector.

at the end can be explained by fraying effects.

Generalized Order Parameters S^2. The correlation functions for internal motions of the proton–proton vectors were calculated from the free dynamics simulation. Correlation functions over 180 ps are shown in Figure 4. Both curves show an initial rapid decay followed by a plateau region, although in Figure 4A there appears to be a further loss of correlation on a longer time scale. Since fast picosecond motions are generally separated from slower dynamic processes, the correlation functions were also calculated for the last nine 20-ps trajectories of the 200-ps dynamics run. Figure 5 shows some interproton internal correlation functions for the time span from 20 to 40 ps. The initial rapid decay is again observed. Furthermore, the plateau value for the correlation function can now be determined better since the slower motions do not play an important role on this time scale.

The first correlation function is for the interproton vector H1′–H4′ for the first residue of the second strand. In this case loss of correlation seems to occur on a time scale of 5–10 ps, and a plateau value is not well-defined but was estimated to be about 0.46. For all the interproton vectors of this residue, the same type of curve as in Figure 5A was observed, giving rise to a low value for the generalized order parameters S^2, which is likely to be caused by the effect of fraying at the end.

The other parts of Figure 5 show correlation functions for interproton vectors of C14, a more rigid part of the DNA. In Figure 5B the correlation function for one of the calibration cross peaks, cytosine H5–H6, is shown. It is not surprising that a very high value of S^2 is observed since the motion of these two protons is highly restricted because of their attachment to the cytosine ring. A different type of interproton vector is that of C14 H6–H2′ in Figure 5C, between a base and a sugar proton. Here the motion is less well correlated, and this is reflected in a lower plateau value ($S^2 = 0.77$). The last curve shown, Figure 5D, is for an interresidue interproton

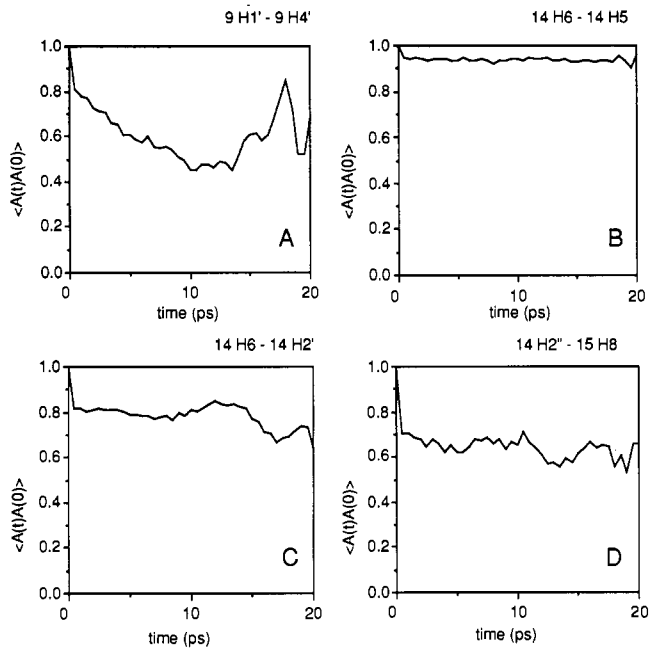

FIGURE 5: Decay for the internal motion correlation function for various interproton vectors for the 20-ps time span. The plateau values corresponding to S^2 are indicated (A) for the intrasugar interproton vector G1 H14'–G1 H1', (B) for the intrabase interproton vector C14 H6–C14 H5, (C) for the intraresidue interproton vector C14 H6–C14 H2', and (D) for the interresidue interproton vector C14 H2''–G15 H8.

vector, C14 H2''-G15 H8. The plateau value is lower again (S^2 = 0.62), indicating that the motional effect is larger than for intraresidue sugar-to-base contacts.

For the other residues in the DNA a similar behavior can be observed. This is true for all the nine subsets of 20 ps. Therefore, the plateau values, S^2, for all nine subsets were averaged and compared with those obtained from the 180-ps time correlation functions. The plateau values for the long trajectory are systematically smaller than the S^2 values found by averaging over the 20-ps subsets. The tendency of highly correlated motion vs lower correlation is, however, preserved. This difference can be due to the fact that at this time scale the slower decay already starts to play a role. Furthermore, the difference in statistics over the time scale (400 time frames for 20 ps vs 3600 time frames for 180 ps) can affect the results of the calculation.

In order to classify different types of contacts, the averaged S^2 values were again averaged but now by grouping them together according to different classes of equivalent interproton vectors. These average values and the standard deviation obtained from averaging are shown in Table I. From Table I it is clear that the interresidue H2''–base(i+1) interproton vector gives rise to the lowest S^2 values. The vectors between the other proton attached to the C2' H2' and the base(i+1) show a slightly higher S^2 value, but it is still lower than the other interresidue sugar–base vectors. For the intraresidue sugar–base vectors the same trend is observed, but in general the plateau values are higher than for the interresidue vectors. All the intrasugar interproton vectors have about the same S^2 value, and these values are comparable to those of intersugar and interbase vectors. Both intrabase vectors are fixed-distance vectors, and therefore it is not surprising that the S^2 values are high.

IRMA Calculations. IRMA calculations were performed by using the same experimental 2D NOE data set as used previously (Boelens et al., 1989). The first structure refinement was done with restrained MD simulations in vacuo. For comparison, the spectral density functions were calculated with and without the effect of local motions as expressed in the order parameters S^2 (eq 4 or 11). The quality of the structures obtained in terms of correspondence with the experimental data set was monitored with the R factor as defined in eq 13. The results are shown in Table II. In all cases the starting structure was the energy-minimized canonical B-DNA. The

Table I: S^2 Values Averaged per Type of Proton–Proton Contact and the Standard Deviation (SD) of These Values

proton–proton contact	S^2	SD
intrabase		
H6–H5	0.92	0.04
H6–Me	0.89	0.08
interbase		
H6/H8–H6/H8(i+1)	0.80	0.07
H6/H8–H5(i+1)	0.80	0.04
H6/H8–Me(i+1)[a]	0.82	0.02
Me–Me(i+1)[b]	0.75	
H2–H2(i+1)[b]	0.63	
sugar–base (intraresidue)		
H1'–H6/H8	0.90	0.04
H1'–H2[a]	0.89	0.01
H2'–H6/H8	0.76	0.09
H2'–H5	0.86	0.05
H2''–H6/H8	0.83	0.07
H3'–H6/H8	0.86	0.08
H4'–H6/H8	0.89	0.05
sugar–base (interresidue)		
H1'–H6/H8(i+1)	0.79	0.09
H1'–H5(i+1)	0.85	0.07
H2''–H6/H8(i+1)	0.60	0.11
H2''–H5(i+1)	0.75	0.09
H2''–Me(i+1)[a]	0.73	0.09
H3'–H6/H8(i+1)	0.82	0.12
sugar–base (interstrand)		
H1'–H2(2,i+1)[a,c]	0.85	0.01
H1'–H2(2,i+1)[a,c]	0.84	0.01
intrasugar		
H1'–H2'	0.80	0.08
H1'–H2''	0.80	0.07
H1'–H3'	0.88	0.03
H1'–H4'	0.81	0.06
H2'–H2''	0.75	0.12
H2'–H3'	0.79	0.11
H2'–H4'	0.86	0.08
H2''–H3'	0.81	0.11
H2''–H4'	0.82	0.10
H3'–H4'	0.82	0.06
intersugar		
H1'–H1'(i+1)	0.81	0.08
H1'–H2(i–1)[a]	0.78	0.08
H2'–H6/H8(i+1)	0.67	0.04
H2'–H5(i+1)	0.74	0.10
H2'–Me(i+1)[a]	0.77	0.05
H1'–H2'(i+1)	0.85	0.06
H1'–H4'(i+1)	0.81	0.05
H2''–H2-(i+1)	0.74	0.10

[a] Averaged over only two of these interproton vectors. [b] Only one of this type of interproton vector. [c] The 2 indicates a residue in the opposite strand.

Table II: R Factors per IRMA Cycle and Distance Restraint Energy E_{dr} (kJ·mol^{-1}·nm^{-2}) for the Starting and Final Structures

	structure[a]			
IRMA cycle	B_R	B_{D1}	B_{D2}	B_{D3}
0 (B-DNA)	0.92	0.67	0.62	0.62
1	0.67	0.54	0.50	0.50
2	0.62	0.51	0.47	0.48
3	0.61	0.50	0.48	0.48
4	0.59	0.50		
E_{dr} (starting)	607	581	521	577
E_{dr} (final)	319	298	274	265

[a] The names of the structures are explained in the text.

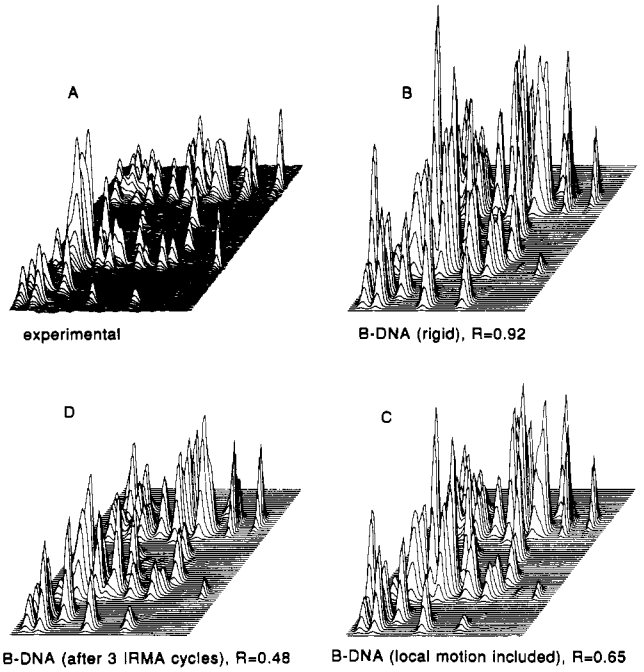

FIGURE 6: Region of the 2D NOE spectrum of the DNA duplex showing cross peaks between the base H6/H8 and sugar H2′/H2″ protons at a mixing time of 176 ms. Shown are (A) the experimental spectrum, the theoretical spectrum based on canonical B-DNA (B) without and (C) with inclusion of fast motion, and (D) the theoretical spectrum based on the refined structure with inclusion of motion.

first column of Table II describes the results for the rigid model [structures $B_R(0)$ to $B_R(4)$]. The R factor for the octamer in the B-DNA conformation (B_R) is 0.92 and decreases to a value of 0.59 after four IRMA cycles. The restraint energy drops from 607 to 319 kJ·mol^{-1}.

Next three IRMA runs were performed by including local dynamics (B_{D1}, B_{D2}, and B_{D3}). For B_{D1}, values for S^2 were taken from the 20–40-ps free MD run discussed above; for B_{D2}, the S^2 values were averages over the nine sets of 20-ps trajectories; while for B_{D3}, the S^2 values were taken as averages for each type of proton pair as shown in Table I. It is clear from Table II that, even with the starting B-DNA structure, the agreement between the experimental and theoretical NOE data is already better as judged from the R factors of 0.67 and 0.65. Again in three or four IRMA cycles converged structures are obtained that have improved R factors in the range of 0.48–0.50. Also the distance restraint energy of these converged structures is substantially lower than that for the starting structures. Structures $B_{D2}(3)$ and $B_{D3}(3)$ appear to be slightly better in terms of R factors and restraint energies (E_{dr}). The fact that the averaged values for S^2 seem to work well is a useful result since it indicates that sequence-dependent effects on local mobilities are not strong. Potentially, therefore, a set of S^2 values could be found that is generally applicable in oligonucleotides of B-DNA-type conformations.

Simulation of the Spectra. In Figure 6 the region of the 2D NOE spectrum containing cross peaks between H6/H8 and H2′/H2″ protons is shown. Figure 6A shows the experimental spectrum at τ_m = 176 ms, while in Figure 6B–D simulated spectra are shown that are scaled to the experimental spectrum with the use of the cytosine H5–H6 cross peaks (outside the displayed region). In Figure 6B the spectrum calculated on the basis of B-DNA by using the rigid-molecule assumption [$B_R(0)$] is shown. It is clear that most of the intense intraresidue base-to-H2′/H2″ cross peaks are too large compared to the experimental ones. However, when local motion is included in the calculation based on the same B-DNA structure, the comparison is already much better (cf. Figure 6C) and improves further after three cycles of IRMA refinement (cf. Figure 6D). This corresponds with the results of the R factor calculation. It is clear that the changes are most pronounced for the peaks for which the S^2 values deviate most from the calibration peaks (S^2 = 0.9).

Table III: R Factors, Distance Restraint Energy E_{dr}, and Total Potential Energy E_{pot} (kJ·mol^{-1}) per IRMA Cycle for the Structures in Water

	structure					
	B-DNA			A-DNA		
IRMA cycle	R	E_{dr}	E_{pot}	R	E_{dr}	E_{pot}
0	0.92	680	−2871	1.09	1666	−2277
1	0.48	321	−3695	0.52	323	−3506
2	0.50	250	−3768	0.54	241	−3896
3	0.49	228	−3697	0.53	234	−3773

Proton–Proton Distance Determination. The IRMA procedure was devised for an accurate determination of proton–proton distances. The question arises: to what extent does the use of the generalized order parameters for inclusion of the local mobility influence the distance determination? On the basis of the ratio of the order parameters for the calibration peaks and those for the other peaks, the approximate changes in distances can be calculated. The largest change, a decrease of about 7%, is expected for the interresidue base-to-H2″ cross peak since the S^2 value was 0.60. Indeed, when the final sets of distances for the rigid run (B_R) are compared with those where internal motion was included (B_D), the largest deviation in distances, a 10% decrease on the average, was observed for the base(i+1)–H2′ cross peak. For all the other proton pairs the changes were smaller, corresponding to the trend in S^2 values.

Structure Determination Starting from A- and B-DNA. We will now discuss the results of calculations following the protocol discussed under Experimental Procedures (cf. Figure 2). The correspondence between the experimental and the theoretical data will be discussed again, but now the structures obtained will be examined in more detail also.

To investigate the convergence of the method, two IRMA refinement runs were carried out starting from energy-minimized canonical A- or B-DNA by using the same set of NOE build-up data as before. Initially the R factors and distance restraint energies are quite high, the R factors being 0.92 and 1.09 and the energies 680 and 1666 kJ·mol^{-1} for the B- and A-DNA models, respectively (see Table III). After 15 ps of restrained MD in water with counterions, the coordinates of the 10-ps trajectories were averaged and energy minimized. Then, free MD simulations were performed with these structures for 42.5 ps to calculate the generalized order parameters (S^2). The obtained S^2 values were similar to the values of Table I (within the standard deviation). NOE intensities calculated with the S^2 values determined for each individual interproton vector for both averaged structures yielded much lower R factors, 0.48 and 0.52, indicating that inclusion of fast internal motion results in a better agreement between calculated and experimental intensitities. Furthermore, it is clear that only after one cycle the A-DNA structure already changed significantly toward a B-like structure that corresponds better with the measured data. The distance restraint energies are also significantly lower and decrease further during two more cycles of IRMA. The R factors improve a little but appear to be less sensitive in this case. For the structure starting from A-DNA, similar values compared to those for the B-DNA derived structure are obtained. The final R factor is 0.49, and the distance restraint energy is 228

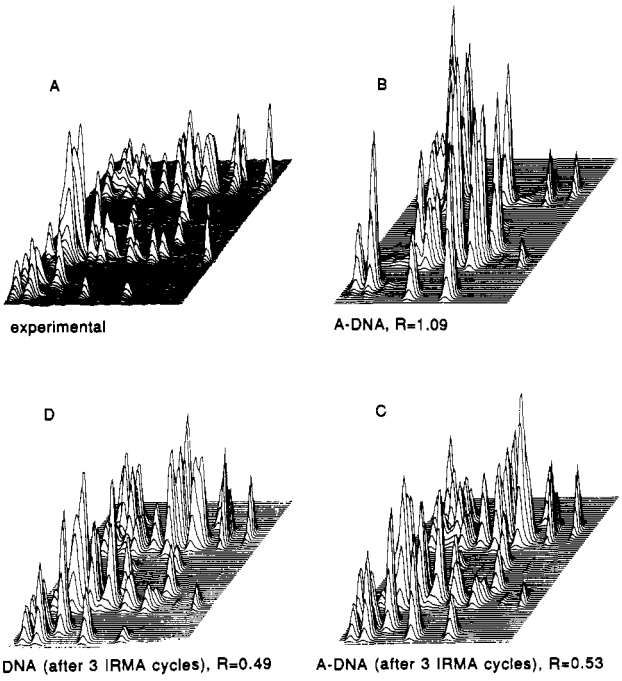

FIGURE 7: Region of the 2D NOE spectrum of the DNA duplex showing cross peaks between the base H6/H8 and sugar H2′/H2″ protons at a mixing time of 176 ms. Shown are (A) the experimental spectrum, the theoretical spectrum (B) without inclusion of motion for a canonical A-DNA structure and with inclusion of motion based on (C) refined A-DNA structure and (D) refined B-DNA structure.

kJ·mol^{-1} for the structure obtained by starting from B-DNA. For the structure obtained by starting from A-DNA the values are 0.53 and 234 kJ·mol^{-1}.

Simulation of the Spectra. Again, as for the in vacuo calculations, the results can be visualized by simulating the NOE spectra and comparing them with the experimental spectrum. This is shown in Figure 7. From this figure it is clear that the A-DNA model (cf. Figure 7B) does not match the experimentally observed spectrum at all. The cross-peak pattern, high intensities for interresidue base-to-H2′ contacts, and very low intraresidue intensities in A-DNA vs high intraresidue and lower interresidue intensities in the experimental spectrum reveal that the DNA molecule adopts a B-DNA-like structure in solution. After three cycles of IRMA both the A- and B-DNA starting structures changed to structures that are in much better agreement with the experimental data. This

Table IV: Root-Mean-Square Difference (Å) of the Structures during the IRMA Cycles

structure	B-DNA	A-DNA	B3	A3
B-DNA		4.2	1.4	3.4
A-DNA			3.6	2.0
B3				2.6
A3				

Table V: Root-Mean-Square Deviations (rmsd) for Superposition of Two Base Pairs at a Time

base pairs	rmsd (Å)	base pairs	rmsd (Å)
GC1–CG2	0.84	TA5–GC6	0.73
CG2–GC3	0.88	GC6–CG7	0.57
GC3–TA4	0.86	CG7–GC8	1.27
TA4–TA5	0.88	⟨average⟩	0.86

was clear already from the *R* factors, but it can also be seen in the simulated spectra of Figure 7C,D.

Convergence of the Structures. In Figure 8 a stereo plot of the two structures obtained from A- and B-DNA starting conformations is shown. From this figure it is clear that in the center of the molecule the structures look alike, but at the ends the structures are diverging. Furthermore, in the A-DNA-derived structure the orientation of the bases is different from the other, which is still reminiscent of the A-DNA starting structure. The root-mean-square difference (rmsd) of the coordinates of the starting models is 4.3 Å, and the effect of refinement on the rmsd can be seen in Table IV. The final difference is 2.6 Å. This is large compared to what is observed for well-refined protein structures, which is not surprising considering the local nature of the distance constraints and the linear character of the DNA duplex, and it can be expected that the convergence at the local level is much better. Indeed, when two base pairs at a time are superimposed, the average rmsd is only 0.86 Å. All these rmsd values are listed in Table V. The effect of local convergence can also be seen in Figure 9 where a stereo plot of the central TT·AA base pairs is shown for both structures. The rmsd for these two base pairs is 0.88 Å.

Analysis of the Structures. In Table VI all the torsion angles are listed for the two structures. Furthermore, the values of the glycosidic angle χ and the sugar backbone torsion angle δ are shown in Figure 10. These two torsion angles are best determined by the NOE constraints since for most residues many intraresidue base-to-sugar and sugar–sugar NOEs were observed. Although in the A-DNA starting structure

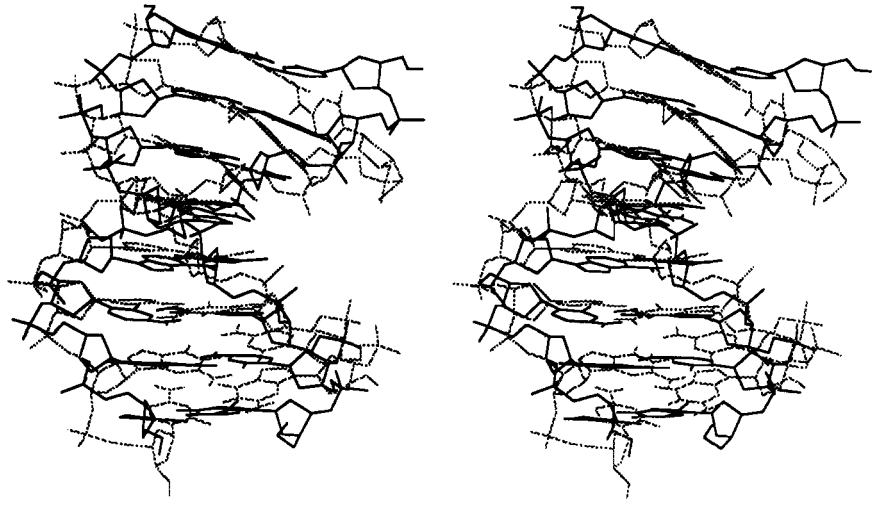

FIGURE 8: Stereopair of the two superimposed structures. The top left is the beginning of the first strand. The solid lines indicate the structure derived from B-DNA, and the dotted grey lines indicate the structure derived from A-DNA.

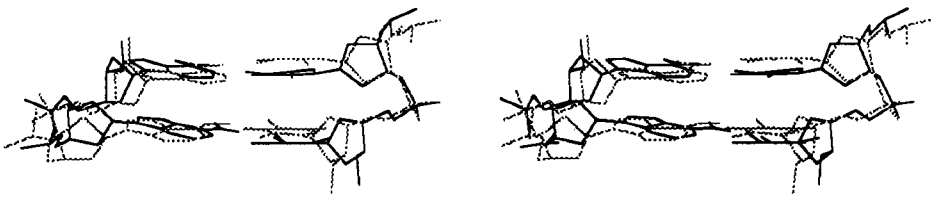

FIGURE 9: Stereopair of the central two base pairs of the DNA octamer for the two superimposed structures. The solid lines indicate the structure derived from B-DNA, and the dotted grey lines indicate the structure derived from A-DNA.

Table VI: Torsion Angles for the Two Final Derived Structures for the DNA Octamer d(GCGTTGCG)·d(CGCAACGC)

	χ		α		β		γ		δ		ε		ζ	
residue	B3	A3	B3	A3	B3	A3	B3	A3	B3	A3	B3	A3	B3	A3
G1	−95	−98					58	57	139	150	169	−176	−96	−100
C2	−112	−119	−65	−75	179	174	61	62	124	118	177	−177	−95	−92
G3	−105	−117	−64	−75	−179	177	58	58	138	133	−179	−172	−94	−99
T4	−108	−113	−82	−82	−172	−174	53	55	124	129	−179	−169	−96	−95
T5	−113	−116	−61	−79	162	170	66	69	123	128	−177	−175	−86	−84
G6	−115	−118	−59	−72	162	175	63	55	117	121	−175	−173	−96	−85
C7	−115	−132	−64	−69	171	165	59	62	114	102	−145	−179	−99	−90
G8	−79	−99	−80	−68	167	178	51	57	130	141				
C9	−134	−122					62	59	80	99	−153	−176	−122	−76
G10	−95	−83	−29	−87	131	−172	59	53	133	136	−178	−177	−105	−101
C11	−109	−113	−72	−69	−177	−167	53	61	119	115	−169	−172	−99	−91
A12	−96	−106	−72	−76	174	−174	56	52	154	139	−66	−169	−178	−100
A13	−101	−111	−103	−82	123	180	61	58	137	133	−169	−175	178	−103
C14	−128	−126	33	−67	74	168	57	69	96	125	−177	−173	−87	−77
G15	−109	−109	−67	−108	172	−179	55	55	126	110	−173	−179	−92	−88
C16	−126	−141	−67	−64	164	164	60	65	115	108				
(average)	−109	−114	−60	−77	158	176	58	59	123	124	−165	−173	−109	−92

structure	χ	α	β	γ	δ	ε	ζ
B-DNA[a]	−117	−63	171	54	123	−169	−108
B-DNA[b]	−102	−41	136	38	139	−133	−157
A-DNA[b]	−154	−90	211	47	83	−175	−45

[a] From the Dickerson dodecamer. [b] From fiber diffraction data.

the values for the glycosidic angle χ are on the average −154°, they change to values in the B-DNA region (−110°). Furthermore, in both structures the same variation in values for this torsion angle can be observed; the same is true for the torsion angle δ (cf. Figure 10b). The H1′–H4′ distance gives a good indication of the sugar conformation. For residues 7 and 14 very short distances were determined, 2.8 and 3.0 Å, respectively, whereas for residue 12 a relatively long distance was derived, 3.5 Å. This distance variation is in agreement with the variation in the torsion angle δ. In structures obtained from X-ray studies (Drew et al., 1981) and also from NMR studies (Clore & Gronenborn, 1985b), a correlation between the glycosidic angle χ and the torsion angle δ was found in B-DNA molecules. For the Dickerson dodecamer the correlation coefficient was 0.78. From Figure 10 it is clear that for our two structures there is a high correlation as well. For the B-DNA-derived structure the correlation coefficient is even higher, 0.83, while for the A-DNA-derived structure it is somewhat less, 0.71. All the other backbone torsion angles are less affected by the NOE constraints, and some more variation in their values is not surprising (cf. Table VI). The average values, however, are close to those observed in the X-ray study of the Dickerson dodecamer. Also for the structure based on the A-DNA starting model, the backbone torsion angles now have values closer to a B-DNA-like structure. For the first structure, B-DNA based, the backbone in the center of the molecule deviates from the average values for the rest of the molecule. This deviation, which was not observed for the second structure, does not affect the structures very much; the rmsd for the two structures in this part is not larger than for any other part. Most likely, the changes compensate each other.

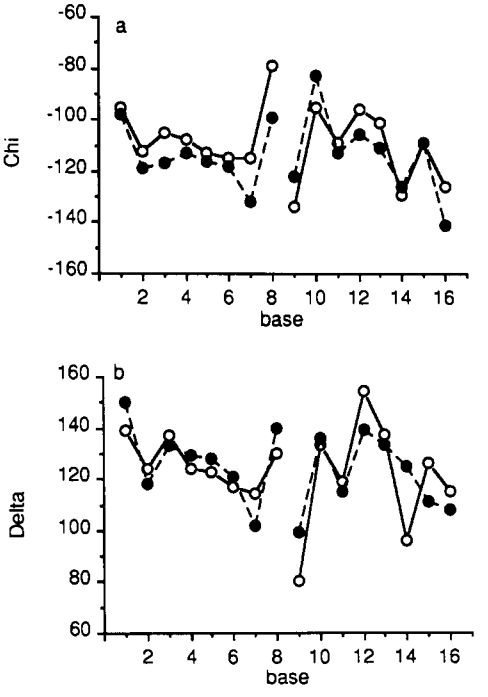

FIGURE 10: (a) The glycosidic torsion angle χ and (b) the sugar backbone torsion angle δ per residue for the two structures. The open circles represent the B-DNA-derived structure, and the filled circles represent the A-DNA-derived structure.

Another well-determined structural parameter is the helical twist. The helical twist angles for both structures obtained are shown in Figure 11a. A small twist for the step from CG2 to GC3 is compensated by a large twist for the step from GC3

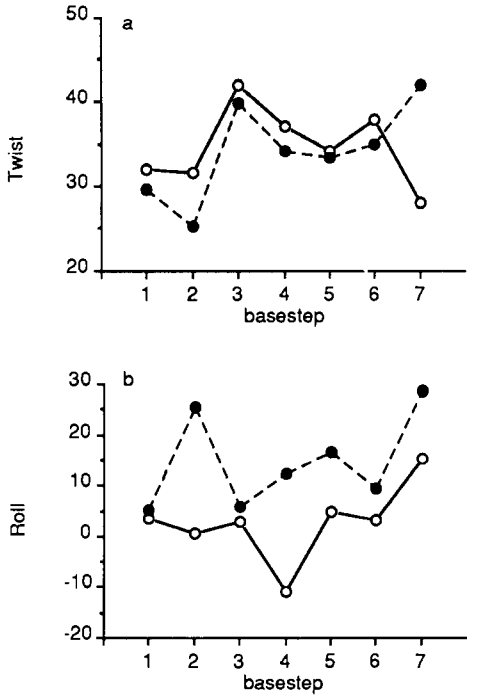

FIGURE 11: (a) The helical twist angles and (b) the base roll angles per base step for the two structures. The open circles represent the B-DNA-derived structure, and the filled circles represent the A-DNA-derived structure.

to TA4. The average twists are 35° and 36° for both models. The sequential NOE between C14 H6 and G7 H1′ is relatively weak (3.6 Å) and is more like what one would observe in A-DNA, where this distance is due to a smaller twist of about 4.0 Å. The next step compensates this small twist angle. The base roll angle is less well determined. Especially for the steps C2 G3 and T4 T5, large differences in the base roll angle can be observed. For the A-DNA-derived structure these are still positive as in X-ray studies of A-DNA (Shakked & Rabinovich, 1986), whereas for the B-DNA-derived structure the base roll angle is around zero, with only a large negative value for the T4 T5 step. As far as the other structural parameters are concerned, such as inclination, displacement, propeller twist, and base-pair opening, the variation along the sequence is the same for both structures, but the average values still resemble those in the starting structures.

When the structure refinement was performed by MD simulations in vacuo, a large kink of the helix axis was observed (Boelens et al., 1989). Calculation of the angle between the helix axes through the first three base pairs and through the last three base pairs reveals that the DNA is still somewhat curved (12° for the B-DNA-derived structure, 30° for the A-DNA-derived structure). However, the curvature is much smoother than in the in vacuo simulations, where the effect of neutralization of the charges on the phosphates may affect the results. Inclusion of the charges on the phosphates for the structures obtained in vacuo results in a 3-fold higher electrostatic energy term compared to the structures simulated in water.

Conclusions

We have made an attempt to include the effect of fast picosecond internal motion of interproton vectors in the iterative relaxation matrix approach for structure determination of biomolecules. This can be conveniently done by using the concept of the generalized order parameter S^2 (Lipari & Szabo, 1982). By lack of information from experiment these S^2 values can be obtained from molecular dynamics simulations. For the present DNA octamer a significant variation of order parameters was observed. For instance, for the interresidue interproton vectors from the H6/H8 to the sugar H2′/H2″ protons, a relatively high mobility and therefore a small order parameter ($S^2 = 0.60$) compared to the other interproton vectors was observed. Our results indicate a dynamic behavior that lies in between the results of Nerdal et al. (1989), who did not find differences in effective correlation times τ_c, and the more extreme differences found by Clore and Gronenborn (1985a). We note, however, that our method only takes into account motions with a picosecond time scale; local mobility with correlation times in the nanosecond range is also known to occur in oligonucleotides [for a review see Kearns (1984)], but cannot be dealt with by the present procedure.

Inclusion of fast local motion in the calculation of cross-relaxation rates and NOE intensities results in a better agreement between the experimental and theoretically calculated spectra. This is clear from a visual comparison between simulated spectra and the experimental spectrum and can also be seen from the R factors, which decrease significantly upon inclusion of these fast internal motions. As far as the NOE distance constraints are concerned, the inclusion of fast local motions gives rise to small differences of the order of 10% at most. These differences, however, appear to be significant since the constraints could be better satisfied as manifested by a lower constraint energy (cf. Tables II and III).

Finally, a protocol is proposed that consists of (1) IRMA without fast internal motions included to determine a first approximate structure, (2) free MD simulation in order to extract the generalized order parameters, and (3) a few more cycles of IRMA with inclusion of motion for further structure refinement. The structures derived with this protocol showed a high local convergence (0.86 Å), but the global convergence was only 2.6 Å. The last value was in the same range as was observed from distance geometry calculations for an eight base pair fragment in a DNA dodecamer by the group of B. R. Reid (personal communication). Recently, Clore et al. (1988) claimed a much higher convergence (0.7 Å) with a similar methodology (restrained MD) for the structure determination, although no correction for spin diffusion was made and the MD simulations were done in vacuo. The reason for this discrepancy is not clear. The method presented here is also applicable to other molecules, such as proteins. An application to a protein structure determination is in progress.

Registry No. d(GCGTTGCG)·d(CGCAACGC), 106931-37-7.

References

Boelens, R., Koning, T. M. G., & Kaptein, R. (1988) *J. Mol. Struct. 173*, 299.

Boelens, R., Koning, T. M. G., van der Marel, G. A., van Boom, J. H., & Kaptein, R. (1989) *J. Magn. Reson. 82*, 290.

Bothner-By, A. A., & Noggle, J. H. (1979) *J. Am. Chem. Soc. 101*, 5152.

Broido, M. S., James, T. L., Zon, G., & Keepers, J. W. (1985) *Eur. J. Biochem. 150*, 117.

Brünger, A. T., Clore, G. M., Gronenborn, A. M., & Karplus, M. (1986) *Proc. Natl. Acad. Sci. U.S.A. 83*, 3801.

Clore, G. M., & Gronenborn, A. M. (1985a) *FEBS Lett. 179*, 187.

Clore, G. M., & Gronenborn, A. M. (1985b) *EMBO J. 4*, 829.

Clore, G. M., & Gronenborn, A. M. (1989) *Crit. Rev. Biochem. Mol. Biol. 24*, 479.

Clore, G. M., Oschkinat, H., McLaughlin, L. W., Benseler, F., Scalfi-Happ, C., Happ, E., & Gronenborn, A. M. (1988) *Biochemistry 27*, 4185.

Drew, H. R., Wing, R. M., Takano, T., Broka, C., Tanaka, S., Itakura, K., & Dickerson, R. E. (1981) *Proc. Natl. Acad. Sci. U.S.A. 78*, 2179.
Fratini, A. V., Kopka, M. L., Drew, H. R., & Dickerson, R. E. (1983) *J. Mol. Biol. 257*, 14686.
Gonzalez, C., Rullmann, J. A. C., Bonvin, A. M. J. J., Boelens, R., & Kaptein, R. (1991) *J. Magn. Reson. 91*, 659.
Jamin, N., James, T. L., & Zon, G. (1985) *Eur. J. Biochem. 152*, 157.
Kaptein, R., Zuiderweg, E. R. P., Scheek, R. M., Boelens, R., & van Gunsteren, W. F. (1985) *J. Mol. Biol. 182*, 179.
Kaptein, R., Boelens, R., Scheek, R. M., & van Gunsteren, W. F. (1988) *Biochemistry 27*, 5389.
Kearns, D. R. (1984) *CRC Crit. Rev. Biochem. 15*, 237.
Keepers, J. W., & James, T. L. (1984) *J. Magn. Reson. 57*, 404.
Kemmink, J., Boelens, R., Koning, T. M. G., Kaptein, R., van der Marel, G. A., & van Boom, J. H. (1987) *Eur. J. Biochem. 162*, 37.
Koning, T. M. G., Boelens, R., & Kaptein, R. (1990) *J. Magn. Reson. 90*, 111.
Lancelot, G., Guesnet, J.-L., & Vovelle, F. (1989) *Biochemistry 28*, 7871.
Lavery, R., & Sklenar, H. (1989) *J. Biomol. Struct. Dyn. 6*, 655.
Lefèvre, J. F., Lane, O. N., & Jardetzky, O. (1987) *Biochemistry 26*, 5076.
Levy, R. M., Karplus, M., & McCammon, J. A. (1981) *J. Am. Chem. Soc. 103*, 994.
Lipari, G., & Szabo, A. (1982) *J. Am. Chem. Soc. 104*, 4546.
Macura, S., & Ernst, R. R. (1980) *Mol. Phys. 41*, 95.
Marion, D., Genest, M., & Ptak, M. (1987) *Biophys. Chem. 28*, 235.
Nerdal, W., Hare, D. R., & Reid, B. (1989) *Biochemistry 28*, 10008–10021.
Nilges, M., Gronenborn, A. M., & Clore, G. M. (1988) *FEBS Lett. 229*, 317.
Olejniczak, E. T., Dobson, C. M., Karplus, M., & Levy, R. M. (1984) *J. Am. Chem. Soc. 106*, 1923.
Olejniczak, E. T., Gampe, R. T., Jr., & Fesik, S. W. (1986) *J. Magn. Reson. 67*, 28.
Pieters, J. M. L., de Vroom, E., van der Marel, G. A., van Boom, J. H., Koning, T. M. G., Kaptein, R., & Altona, C. (1990) *Biochemistry 29*, 788.
Rullmann, J. A. C., Lamerichs, R. M. J. N., Gonzalez, C., Koning, T. M. G., Boelens, R., & Kaptein, R. (1990) Proceedings of the 44th International Meeting of the Division de Chimie Physique (Societé Française de Chimie), Nancy, France.
Shakked, Z., & Rabinovich, D. (1986) *Prog. Biophys. Mol. Biol. 47*, 159.
Solomon, I. (1955) *Phys. Rev. 99*, 559.
States, D. J., Haeberkorn, R. A., & Ruben, D. J. (1982) *J. Magn. Reson. 48*, 286.
Summers, M. F., South, T. L., Kim, B., & Hare, D. R. (1990) *Biochemistry 29*, 329.
Tidor, B., Irikura, K. K., Brooks, B. R., & Karplus, M. (1983) *J. Biomol. Struct. Dyn. 1*, 231.
Van Boom, J. H., van der Marel, G. A., van Boekel, C. A. A., Wille, G., & Hyuong, C. F. (1982) in *Chemical and Enzymatic Synthesis of Gene Fragments*, p 53, Verlag Chemie, Weinheim, Germany.
Van der Marel, G. A., van Boekel, C. A. A., Wille, G., & van Boom, J. H. (1981) *Tetrahedron Lett. 22*, 3887.
Van Gunsteren, W. F., & Berendsen, H. J. (1987) *GROMOS library manual*, Biomos BV, Nijenborgh 16, Groningen, The Netherlands.
Van Gunsteren, W. F., Berendsen, H. J. C., Geurtsen, R. G., & Zwinderman, H. R. J. (1986) *Ann. N.Y. Acad. Sci. 84*, 287.
Woessner, D. E. (1962) *J. Chem. Phys. 36*, 1.
Wüthrich, K. (1986) *NMR of Proteins and Nucleic Acids*, John Wiley and Sons, New York.
Wüthrich, K. (1988) *Science 243*, 45.